Analytical Study of Optical SSB-DMT with IMDD

Amin Yekani, Siamak Amiralizadeh, and Leslie A. Rusch

IEEE/OSA Journal of Lightwave Technology, (Volume 36, Issue 3) (2018)

Doi: 10.1109/JLT.2017.2775183

https://ieeexplore.ieee.org/document/8114164/

Analytical Study of Optical SSB-DMT with IMDD

Amin Yekani, *Member, IEEE,* Siamak Amiralizadeh, and Leslie A. Rusch, *Fellow, OSA*, *Fellow, IEEE*

***Abstract*—We theoretically study the performance of single sideband discrete multi-tone (SSB-DMT) in the C-band with intensity modulation and direct detection (IMDD). Our analysis allows us to quantify the impact of different noise sources such as signal-to-signal beating interference, phase-to-amplitude noise, attenuation, and receiver sensitivity on SSB-DMT. Our analytical tools also allow us to optimize the signal-to-carrier power ratio to maximize SSB-DMT throughput. We provide equations to calculate bit error rate of bit allocated SSB-DMT. Finally we examine various system parameters (laser linewidth, system bandwidth, and fiber length) to determine their impact on the performance of zero guard band SSB-DMT.**

***Index Terms*—SSB-DMT, laser linewidth, fiber length, transmission rate, bandwidth, signal-to-signal beating interference, phase to amplitude noise, inter-carrier interference, signal-to-carrier power ratio.**

I. Introduction

HIGH speed video streaming, social networking, and cloud services are driving 400 GbE standardization. Data centers ($\leq$10 km) and passive optical networks ($\leq$40 km) will require 400 Gb/s transmission at low complexity and cost. Discrete multi-tone (DMT), because of its high throughput and compatibility with intensity modulation and direct detection (IMDD), is one of the most promising modulation schemes for these short reach applications.

Recently various experimental demonstrations have witnessed more than 100 Gb/s data transmission with DMT, such as our previous work on an O-band SiP modulator at 120 Gb/s [1], 130 Gb/s DMT transmission using SiP modulator in the C-band (1550 nm) [2], etc. In this paper we provide tools to predict the performance of DMT in different system parameters (laser linewidth, fiber length, bandwidth, and signal-to-carrier power ratio). We focus on SSB-DMT in the C-band however, our analysis could be also used for DMT in the O-band.

C-band has nonzero chromatic dispersion in single mode fiber (SMF), which causes inter-symbol interference and power fading. Power fading can be bypassed for DMT when using single sideband (SSB) modulation. Both our analysis and simulation assumes ideal SSB-DMT. SSB-DMT can be created by filtering one sideband or via dual drive Mach-Zehnder modulator (DDMZM) [3]; the second choice suffers no distortion from non-ideal filtering.

When chromatic dispersion in C-band combines with phase noise in the optical source (especially when using low cost, large linewidth lasers) other noise sources are introduced to SSB-DMT, such as inter-carrier interference (ICI), phase rotation (PR), and phase-to-amplitude (P2A) noise. Our semi-analytical model for DMT performance in the C-band takes all these noise sources into account.

The effect of phase noise combined with fiber chromatic dispersion was studied previously for uniform SSB-DMT with the assumption of zero padding half of the sub-carriers to avoid generation of signal-to-signal beat interference (SSBI) [4]. This assumption eases analysis, but cuts the achievable transmission rate by half. To achieve more spectral efficiency, we assume zero guard band. There are many SSBI compensation techniques. One example is the Krames-Kronig method and 4x oversampling [5], [6], or using receiver-based two-stage linearization filter [7], or other digital signal processing (DSP) based methods in [8]–[10]. Hardware cancellation techniques based on balanced receivers [11], [12] can be used in the optical domain. Such techniques increase complexity, thus we focus instead on mitigating SSBI by controlling signal-to-carrier power ratio (SCR or γ^2).

P2A noise has been studied before for the case of on-off keying (OOK) modulation [13], however, to the best of our knowledge there is no study of its effect on DMT. We examine the relative importance of P2A and SSBI to overall performance as SCR varies. Increasing SCR decreases SSBI but at the same time it increases P2A noise, making it non-negligible.

This paper starts with a mathematical model of DMT in section II, where all noise contributions in DMT are identified. In section III the DMT noise sources are studied in detail to estimate SNR per subchannel in the presence of laser phase noise and chromatic dispersion. The estimate of cumulative (from all noise sources) SNR per subchannel is compared with SNR per subchannel prediction from Monte Carlo simulation with good agreement. In section IV, results from section III are used to find the signal-to-carrier power ratio (SCR) yielding an SNR distribution per subchannel leading to optimal DMT performance. The optimal DMT operating point (i.e. the best SCR) is used in section V, where we demonstrate the performance of DMT in different system parameters. Finally, some concluding remarks are made.

II. System Model for SSB-DMT

In this paper we use the model in [4] for our single-polarization, uniform SSB-DMT signal. Our only modification is removing the frequency gap between signal and carrier (i.e., we set $N_d = N$ where N_d is the number of data carrying subchannels in [4]), allowing us to study the SSBI effect. The launched SSB-DMT signal in the time domain is

$$s_{DMT}(t) = A_c e^{j2\pi(f_c)t + j\Phi(t)} \left(1 + \gamma \sum_{k=1}^{N} p_k d_k e^{(j2\pi k \Delta f)t}\right), \quad (1)$$

where $s_{DMT}(t)$ is the DMT signal in time domain, A_c is the carrier amplitude, f_c is the carrier frequency, γ^2 is the signal-to-carrier power ratio (SCR), p_k and d_k are the allocated power and normalized complex amplitude of the k^{th} subchannel, respectively, N is the number of subchannels, and Δf is the subchannel frequency spacing. Laser phase noise, $\Phi(t)$, with linewidth of $\Delta\nu$, is modeled by a Wiener process. Let

$$T_k = [cDLk\Delta f/f_c^2] \tag{2}$$

be the time delay or the walk-off for the k^{th} subchannel, in which D is dispersion, L is fiber length, and c is the speed of light in a vacuum. Fiber chromatic dispersion is modeled in the time domain by a delta function $\delta(t-T_k)$, applicable to a single subchannel.

Taking into account laser phase noise and fiber chromatic dispersion, the received signal modulating the optical carrier ($e^{j2\pi f_c t}$), can be modeled as

$$\begin{aligned} r(t) &= \sum_{k=-\infty}^{\infty} A_c e^{j\Phi(t)} * \delta(t-T_k) \\ &+ A_c e^{j\Phi(t)} \gamma \sum_{k=1}^{N} p_k d_k e^{j2\pi k\Delta f t} * \delta(t-T_k) \end{aligned} \tag{3}$$

The first term is the impact of fiber dispersion on carrier phase noise, which will create phase-to-amplitude (P2A) noise after square-law photo detection. This has been studied previously for OOK in [13]. In section III.B we extend that previous OOK study the uniform SSB-DMT case.

By assuming that the laser linewidth is smaller than the frequency spacing of one subchannel, the second term of (3) can be approximated by

$$\begin{aligned} &A_c e^{j\Phi(t)} \gamma \sum_{k=1}^{N} p_k d_k e^{j2\pi k\Delta f t} * \delta(t-T_k) \\ &\approx A_c \gamma \sum_{k=1}^{N} p_k d_k e^{j2\pi k\Delta f (t-T_k) + j\Phi(t-T_k)}, \end{aligned} \tag{4}$$

This assumption is reasonable even for the worst case we examine where the overall frequency occupation is more than 10 GHz, the number of subchannels is $N = 512$, hence $\Delta f \geq 19.5$ MHz, and our laser linewidth $\Delta\nu$ is less then 2 MHz.

After square-law photodetection, the output signal is

$$\begin{aligned} &\left(2P_c Re\left[\gamma \sum_{k=1}^{N} p_k d_k e^{j2\pi k\Delta f t + j\rho_k(t) + j\theta_k} \right] \right. \\ &\left. + \left[P_c \gamma^2 \sum_{k=1}^{N} |p_k.d_k|^2 \right] + P2A + SSBI \right), \end{aligned} \tag{5}$$

where $P_c = |A_c|^2$ is carrier power, $\rho_k(t) = [\Phi(t-T_k) - \Phi(t)]$ is phase fluctuation on kth subchannel, and $\theta_k = -2\pi k\Delta f T_k$. The first term in (5) is the SSB-DMT signal distorted by ICI, PR, and power degradation. The second term is a DC offset.

The third term in (5), as mentioned earlier, is the carrier self-interference which we call P2A noise, this term can be expressed as

$$\begin{aligned} P2A = A_c^2 \sum_{k=-\infty}^{\infty} \sum_{j=-\infty}^{\infty} & e^{j\Phi(t)} * \delta(t-T_k) \times \\ & e^{j\Phi(t)} * \delta(t-T_j). \end{aligned} \tag{6}$$

We analyze P2A noise in section III.A. The last term in (5) is the signal self-interference in the form of SSBI which is created by subchannels beating against one another, and we analyze this contribution in section III.B The SSBI term is not affected by phase noise or chromatic dispersion. Note that P2A was neglected in previous works with zero padding of half the available subcarriers where systems operate in the high SCR regime. We will see in the next section that without that assumption, P2A noise can dominate for low signal-to-carrier power ratios.

III. Validation of Theoretical SNR Prediction

In this section we estimate SNR per subchannel of uniform SSB-DMT ($p_k = 1$) and validate our results via Monte Carlo simulation. The SNR estimates are the basis for determining non-uniform DMT performance using water-filling techniques in section IV and V.

In the appendix A we describe a numerical simulation model for estimating SNR per subchannel using Monte Carlo techniques. By its nature, the SNR estimates include the cumulative effect of all noise sources. Figures in this section include Monte Carlo results (cumulative effect of noise) and analytical results (contribution of each independent noise).

In this section we individually analyze each noise contribution in turn. For different signal-to-carrier ratios, the relative importance of each noise source varies. We examine several SCR regimes where different noises dominate.

Analysis in [13] found an expression for P2A noise power spectral density (PSD), which was used to find P2A noise for OOK. In Section III.A we find P2A noise power for SSB-DMT using this P2A PSD. Section III.B presents new analysis of SSBI noise. Section III.C recalls results from [4] on the interaction dispersion with phase noise. Section III.D combines results from previous subsections into a prediction of overall SNR. Finally, in section III.E we show the average SNR (across subchannels) is a good figure of merit for optimizing SCR.

A. Phase to Amplitude Noise

In 5 the phase-to-amplitude (P2A) degradation depends on the carrier, not the signal. The binary OOK signal analysis of P2A noise [13] is extended here to DMT signals, to the best of our knowledge for the first time. As in [13], we use a Bessel expansion of the electrical field and neglect contributions from

the higher order terms. The power spectral density of P2A noise is

$$PSD_{P2A}(f) \approx \frac{1}{2}\left[\sum_{n=0}^{\infty} 4J_n\left(\frac{1}{f}\sqrt{\frac{2\Delta\nu}{\pi}}\right) J_{n+1}\left(\frac{1}{f}\sqrt{\frac{2\Delta\nu}{\pi}}\right) \times \sin\left\{\frac{1}{2}(2n+1)(2\pi f)^2 k'' L\right\}\right]^2, \tag{7}$$

where J_n is the n^{th} order Bessel function of the first kind, L is the fiber length, and $k'' = \frac{\lambda^2}{2\pi c}D$, where c is the speed of light. The P2A noise power is the product of the carrier power and P2A PSD.

To calculate SNR for the k^{th} subchannel we find subchannel noise power $\sigma^2_{k(P2A)}$ and signal power $\sigma^2_{k(S)}$ by

$$\sigma^2_{k(P2A)} = P_c \int_{(k-1)\Delta f}^{k\Delta f} PSD_{P2A}(f)df, \tag{8}$$

$$\sigma^2_{k(S)} = \frac{P_s}{N_s} = \frac{\gamma^2 P_c}{N_s}, \tag{9}$$

where N_s is the number of subchannels with data, P_s is the overall signal power, and γ^2 is the signal-to-carrier power ratio. Finally, the SNR per subchannel for P2A noise is

$$SNR_{k(P2A)} = \frac{\sigma^2_{k(S)}}{\sigma^2_{k(P2A)}}. \tag{10}$$

To validate (10), we vary SCR and compare Monte Carlo (MC) simulations of SNR per subcarrier (see appendix A) with theoretical predications from (10). Results are presented in Fig. 1 for fiber length of 20 km, signal bandwidth of 32 GHz, and laser linewidth of 100 kHz. Two abscissa axes are provided, the lower one for subcarrier number, and the upper one for frequency. The MC simulation (solid lines) take into account all noise sources.

In Fig. 1a we vary SCR γ^2 from -30.5 dB to -22.5 dB; theoretical results (dotted lines) include only P2A noise. For low SCR, P2A-only theory matches the all-noise simulation (solid lines). However, as the signal-to-carrier power ratio increases, the two begin to diverge. We conclude that at low SCR the P2A noise dominates, but other noise sources take over as the signal power grows. We next examine those other noise sources.

B. Signal to Signal Beating Interference (SSBI)

The last term in (5), SSBI, shows the effect of subchannels beating against one another instead of the carrier. This effect can be calculated as

$$\sigma^2_{k(SSBI)} = \frac{1}{P_c}\sum_{n=-N}^{N} \sigma^2_{n(S)}\sigma^2_{k-n(S)}, \tag{11}$$

more details for (11) are provided in appendix B. The SNR per subchannel is calculated by

$$SNR_{k(SSBI)} = \frac{\sigma^2_{k(S)}}{\sigma^2_{k(SSBI)}}. \tag{12}$$

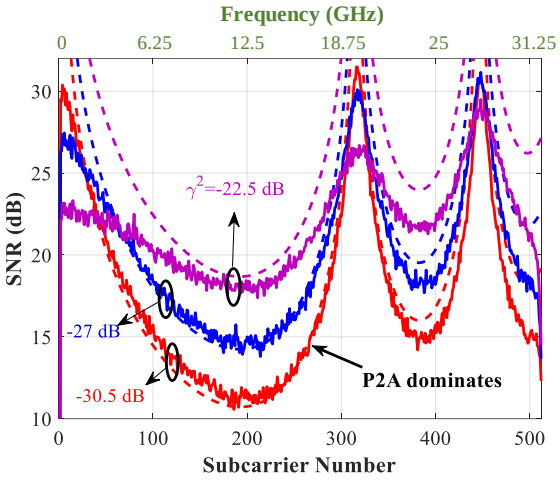

(a)

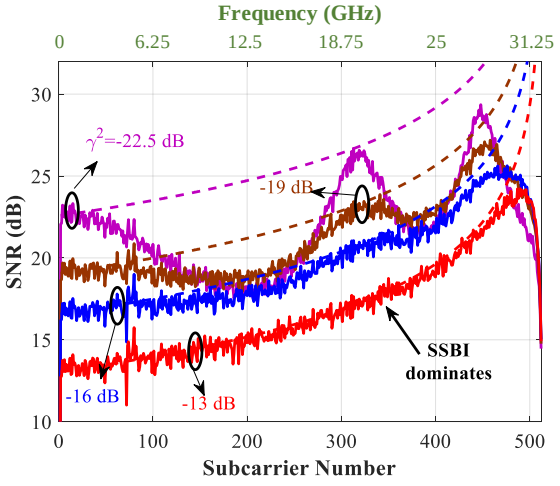

(b)

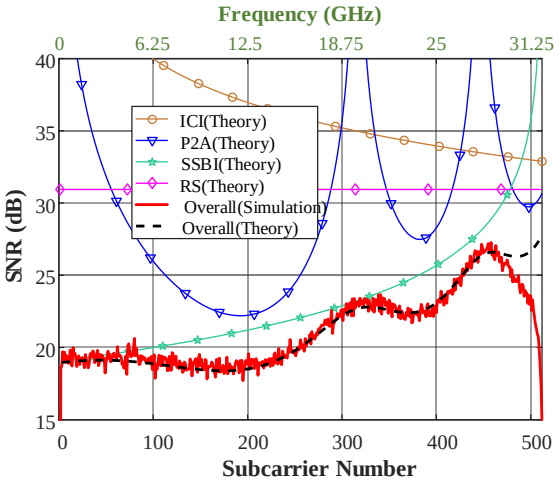

(c)

Fig. 1. SNR per subchannel is found for 20 km of fiber, 32 GHz signal bandwidth, and 100 kHz laser linewidth. Monte Carlo simulation of all noise sources is shown in solid lines, theoretical SNR predictions are shown in (a) for P2A only (dashed) for three values of γ^2; (b) for SSBI only (dashed) for three values of γ^2; and (c) for $\gamma^2 = -23$ dB for each noise source separately (see markers), and all noise sources (black dotted).

As γ^2 grows, so does the signal power $\sigma^2_{k(S)}$, and SSBI as well. From (10), increasing SCR γ^2 leads to lower $SNR_{k(P2A)}$, leading to SSBI to dominate after a threshold value for signal-to-carrier power ratio.

In Fig. 1b we vary γ^2 from -22.5 dB to -13 dB, and theoretical results from (12) (dotted lines) include only SSBI noise. Comparing all-noise Monte Carlo simulation and SSBI-only theory we see that for SCR greater than -16 dB, SSBI is the dominant noise source.The parameter γ^2 affects both P2A and SSBI, but in opposite ways.

C. Interaction of dispersion with phase noise

In (5), the first term describes the interaction of dispersion with phase noise. This interaction leads to these effects: 1) power degradation α, 2) intercarrier interference (ICI), and 3) phase rotation (PR). These degradations were studied in uniform SSB-DMT where half the subchannels (those near the carrier) were used as a guard band to eliminate SSBI [4]. Using this results with zero guard band ($N_d = 0$), the power degradation of the k^{th} subchannel due to phase noise is

$$\alpha_k \approx 1 - 2\pi\Delta\nu T_k = 1 - \beta_k, \tag{13}$$

where $\beta_k = 2\pi\Delta\nu T_k$ is the phase noise power in the k^{th} subchannel.

The variance of the ICI for k^{th} subchannel is

$$\sigma^2_{k(ICI)} \approx \frac{\beta_k}{N^2}\left(N^2 + \frac{1}{3}M_k^2 - NM_k - \frac{1}{3}\right), \tag{14}$$

where T_s is the sampling interval of the DAC and $M_k = T_k/T_s$ is the delay relative to the carrier (in number of samples) for the k^{th} subchannel.

The PR variance for the k^{th} subchannel is

$$\sigma^2_{k(PR)} \approx \frac{\beta_k}{3N^2}\left(-M_k^2 + 3NM_k + 1\right), \tag{15}$$

The PR variance is essential in the calculation of symbol error rate from estimated SNR described in appendix C. However, the impact of PR on the subcarrier SNR itself is negligible as the sum of ICI and PR variances is dominated by the ICI variance. To see this, we note that the ratio of PR variance to ICI variance decreases with increasing fiber length or decreasing FFT size. For 50 km fiber and typical FFT size of 1024, that ratio is less than -32 dB. This small value justifies writing the SNR per subchannel for the first term of (5) as

$$SNR_{k(ICI)} = \frac{\alpha_k}{\sigma^2_{k(ICI)} + \sigma^2_{k(PR)}} \approx \frac{\alpha_k}{\sigma^2_{k(ICI)}}. \tag{16}$$

D. Overall SNR

In this section we combine the effect of all noise sources using superposition law as

$$\begin{aligned}\frac{1}{SNR_k} =& \frac{1}{SNR_{k(ICI)}} + \frac{1}{SNR_{k(P2A)}} \\ &+ \frac{1}{SNR_{k(SSBI)}}. + \frac{1}{SNR_{k(RS)}},\end{aligned} \tag{17}$$

where $SNR_{k(RS)}$ captures the effect of receiver sensitivity and is a white process with the same noise power for all subchannels. In (17) we assumed that the effects of different noise sources on each other are negligible and that they may be considered independent. A final simulation was run to validate this assumption.

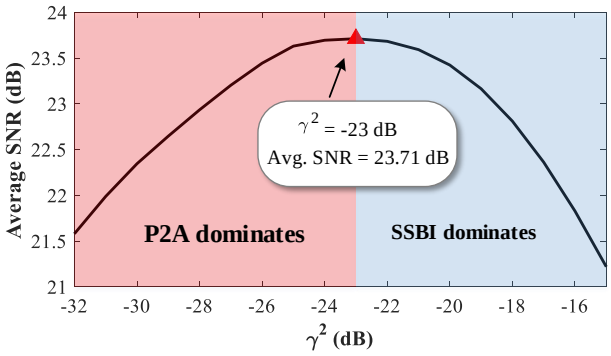

Fig. 2. Average SNR over subchannels for different values of γ^2.

Figure 1c shows the SNR from each noise source separately: ICI with circle markers, P2A with triangles, SSBI with stars and RS with diamonds. The dashed line is the total SNR predicted by (17). As can be seen, the theoretical total SNR matches well the MC simulated SNR per subcarrier. In the case of bandlimited channel, the overall SNR per subchannel would, of course, also be affected by the channel frequency response.

IV. Optimal SCR for DMT

The performance of DMT is determined by the SNR distribution per subcarrier, which is influenced by SCR. To justly compare PAM and DMT, we use our SNR prediction per subcarrier to select the most beneficial operating point for DMT, that is, the optimal signal-to-carrier ratio γ^2. BER is the most appropriate optimality criterion, but requires excessive calculation and results will vary depending on the DMT bit and power allocation algorithm used. We compare SCR minimizing BER under Chow's algorithm with SCR maximizing the average SNR. We will find that optimal SCR under the two criteria are very close (within ~ 1 dB).

A. SNR averaged over subchannels

From the total SNR per subchannel, the SNR averaged over subchannels can be found as a function of SCR. Figure 2 plots average SNR versus SCR. Once again, results are for fiber length of 20 km and laser linewidth of 100 kHz, but no bandwidth limit. This figure shows that for $\gamma^2 < -23$ dB P2A noise dominates, while above that threshold, SSBI dominates. For Fig. 2, receiver sensitivity was an additive white Gaussian noise (AWGN) with $SNR_{RS(B2B)} = 35$ dB to focus on other degradation sources. However, in subsequent estimations we use a more practical value typical for photodetection; $SNR_{RS(B2B)} = 22$ dB for the balance of the paper.

We next systematically examine the three system parameters that affect the SNR averaged over subchannels: laser linewidth, fiber length and system bandwidth. The average SNR in dB

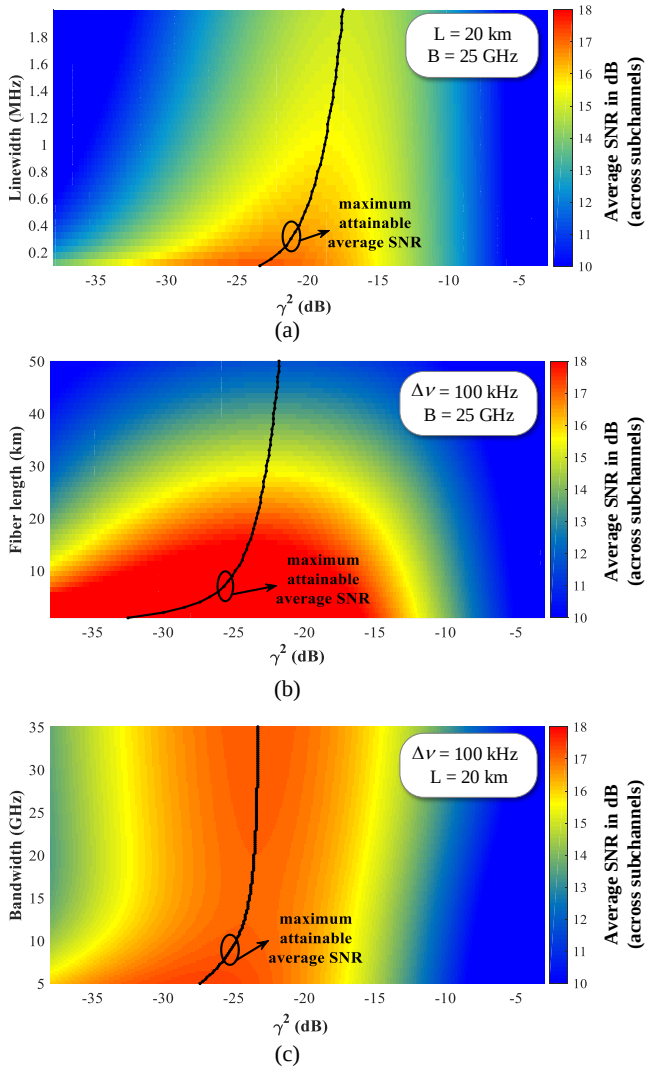

Fig. 3. Average SNR in dB for different values of γ^2 and different values of a) laser linewidth, b) fiber length, and c) channel bandwidth. Black curves show the maximum attainable average SNR in each case.

(a 2D color map) as a function of γ^2 over the range -38 dB to -3 dB is found for each parameter in turn in three plots.

Figure 3a shows average SNR for linewidth from 100 kHz to 2 MHz. For this plot the fiber length is 20 km and system bandwidth is 25 GHz. The black line traces the optimum SCR as a function of linewidth, ranging from -23 dB for narrow linewidth to -18 dB at 2 MHz linewidth.

Figure 3b holds linewidth at 100 kHz and system bandwidth at 25 GHz, and varies fiber length from 0 km (back-to-back or B2B) to 50 km. Again, optimum SCR is traced in the black line, ranging from -33 dB for B2B to -23 dB at 50 km.

Finally, Fig. 3c holds fiber length to 20 km and linewidth to 100 kHz, and examines system bandwidth. As bandwidth changes from 5 GHz to 35 GHz the optimum value for signal-to-carrier power ratio ranges from -27 dB to -23 dB. Comparing the three plots in Fig. 3, average SNR and optimum SCR is more sensitive to fiber length than linewidth or bandwidth.

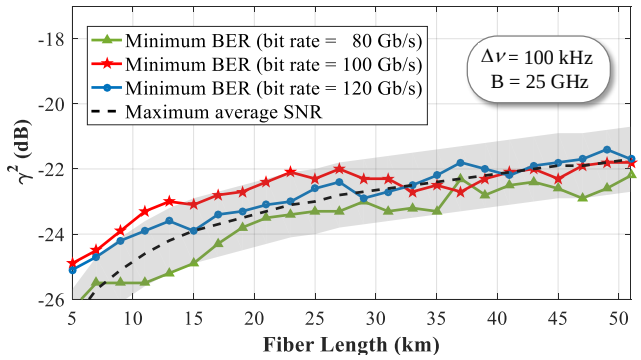

Fig. 4. Optimized γ^2 which maximizes average SNR (dotted line) and when it minimizes BER for three different bit rates 80, 100, and 120 Gb/s (solid lines) versus fiber length.

B. DMT BER calculation

We calculate DMT performance using the theoretical estimation of SNR per subchannel from the previous sections for a given linewidth $\Delta\nu$, fiber length L and system bandwidth B. This SNR per subchannel is used to find the bit and power allocation for DMT using Chow's margin adaptive algorithm [14]. This water-filling algorithm starts with bit allocation (for the given SNR per subchannel) to achieve a target bit rate. The second step is calculating the required power allocation for each subchannel to achieve a target BER with the bit allocation. Certain combinations of bit rate and bit error rate will be achievable for a given SNR distribution, while others will not. Note that Chow's algorithm uses a strict Gaussian noise assumption to determine the bit and power allocations.

Once the bit and power allocations are determined, we calculate the overall BER using equations developed in appendix C that include phase rotation effects (not considered in Chow's algorithm). For a given subcarrier, the bit allocation determines the MQAM constellation used, and (17) gives the SNR for the additive white Gaussian noise. The phase rotation (PR) is a non-additive Gaussian noise. The SER can be found when conditioned on the PR, and then averaging over the PR probability density function. The SER calculation is based on each QAM constellation point falling into one of three categories, depending on its number of nearest neighbors. We find the SER for each category, and then the total SER in the presence of AWGN and PR. Finally, we assume Grey coding to find the BER.

C. DMT Optimization

Using this technique for BER calculation we can sweep SCR and find the optimum SCR that minimizes BER. We compare the optimum SCR when minimizing BER vs. maximizing average SNR in Fig. 4. The SCR maximizing average SNR is given by a black dashed line. As the BER will vary with bit rate, we examine three rates: 80, 100 and 120 Gb/s whose optimal SCR is traced by green, red, and blue solid lines, respectively. The optimum SCR varies with the triplet (L, $\Delta\nu$, B). In Fig. 4, fiber length as an example of triplet is swept, while the two others are held constant. Same analysis is

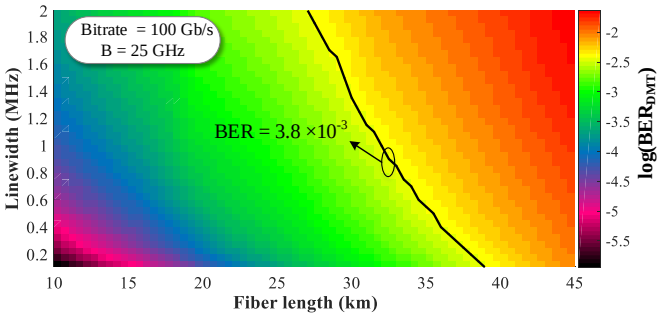

Fig. 5. BER of SSB-DMT for different laser linewidth and fiber length. (Channel bandwidth = 25 GHz)

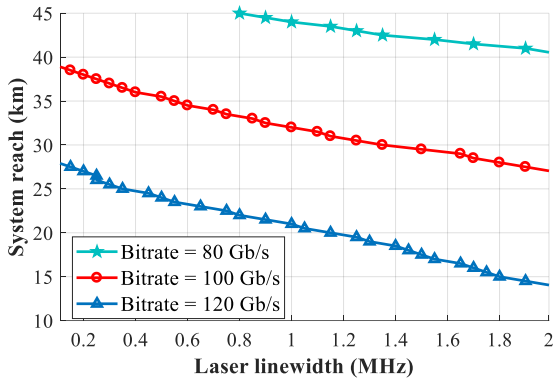

Fig. 6. System reach at BER = 3.8×10^{-3} of SSB-DMT for different laser linewidth.

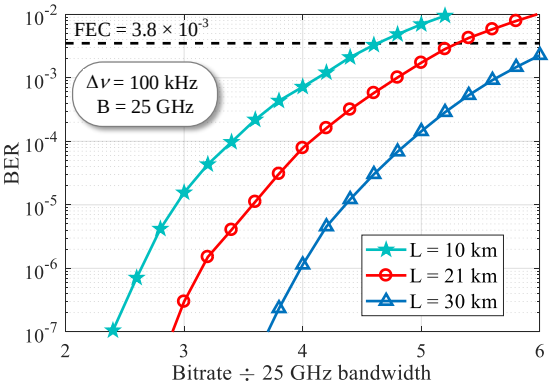

Fig. 7. BER versus spectral efficiency. (Channel bandwidth = 25 GHz, and $\Delta\nu$ = 100 kHz)

done for linewidth and bandwidth. The grey region represents the zone within 1 dB on either side of the curve for SCR maximizing average SNR.

In all cases changing bit rate does not have much effect on the value of optimized SCR, i.e., the curves are clustered in all plots. We also observe that SCR for minimum BER falls within or very close to the gray region. That is, that the two optimality criteria result in an optimal SCR that is similar (to within $\sim$ 1 dB). Optimizing signal-to-carrier power ratio by maximizing average SNR is much less compute intensive than minimizing BER. In the next section, DMT performance is found with SCR optimized for maximum average SNR.

V. Impact of System Parameters on SSB-DMT

In this section we use our analytical tool to study the performance of SSB-DMT in a variety of operational constraints examining the triplet of fiber length, linewidth, and channel bandwidth (L, $\Delta\nu$, B), as well as the bit rate.

A. Impact of Fiber Length and Linewidth

We study the joint effect of fiber length and laser linewidth on SSB-DMT. Figure 5 shows via color map, the logarithm of SSB-DMT BER for fiber length 10 to 45 km and linewidth from 0.1 to 2 MHz. Bandwidth is held at 25 GHz and the bit rate is 100 Gb/s. The ordered pairs of fiber length and laser linewidth leading to BER = 3.8×10^{-3} are given in the black line. This figure shows that the system reach (maximum fiber length with BER under FEC threshold) for the case of a costly, high quality laser with linewidth of 100 kHz is almost 40 km; with a lower quality laser with linewidth of 2 MHz, we can still achieve 30 km reach.

System reach is also calculated for bit rates of 80, 100, and 120 Gb/s in Fig. 6. Increasing bit rate will force the DMT waterfilling technique to choose higher order QAM, which is more sensitive to noise, thus decreasing system reach. This figure shows that the system reach of 80 Gb/s SSB-DMT is always greater than 40 km, even when using a lower cost laser with linewidth of 2 MHz. When increasing the bit rate to 120 Gb/s, system reach is limited to 27 km for the best case of laser linewidth 0.1 MHz.

B. Impact of Bandwidth Constraints

In this section, we assume a fixed hardware solution limiting the channel bandwidth to 25 GHz, and we vary the bit rate. This bandwidth represents current limits of commercially available integrated coherent receivers. We present BER results as a function of spectral efficiency (the ratio of bit rate to system bandwidth). A lower ratio corresponds to less aggressive bit rates for a given hardware solution, while a higher ratio corresponds to aggressively pushing high bit rates through a restricted bandwidth. We selected the case of 10, 21, and 30 km fiber length and 100 kHz laser linewidth for our performance analysis.

Figure 7 shows the BER of SSB-DMT versus spectral efficiency. Fiber length influences several noise terms in the SNR per subcarrier, leading to a complex effect on DMT performance. In addition, DMT performance changes markedly as we change bit rates (see spread of each curve in Fig. 7). This performance analysis shows that when the fiber length is 10 km the maximum bit rate for BER less than FEC is $4.5 \times 25 = 112.5$ Gb/s; if we increase fiber length to 21 and 30 km, the maximum bit rates with BER under FEC threshold are 130 Gb/s and more than 150 Gb/s, respectively.

VI. Conclusion

We presented a theoretical analysis to study the performance of SSB-DMT. Such an analysis requires that SSB-DMT be

optimized, particularly with respect to the signal to carrier ratio. Our tools allows this optimization. Using our analytical tools, we simulated the impact of hardware-imposed bandwidth limitation on SSB-DMT. Our results can be used to select to select appropriate hardware (modulators and laser sources), or to quantify attainable bit rates or system reach.

APPENDIX A
SIMULATION OF UNIFORM SSB-DMT TRANSMISSION AND SNR ESTIMATION

Figure 8 shows the simulation setup and digital signal processing (DSP) flowchart for uniform SSB-DMT transmission. The transmitter side DSP generates a pseudo-random binary sequence (PRBS) that is modulated onto complex QAM symbols for single sideband uniform DMT. The frequency domain signal is converted to the time domain via the inverse fast Fourier transform (IFFT) with size equal to twice the number of subchannels. To remove dispersion induced inter-symbol interference (ISI), a sufficiently long cyclic prefix is added to the signal. Parallel-to-serial conversion, clipping and quantization are the last DSP blocks.

The digital to analog converter (DAC) is simulated as an 8-bit quantization at 64 GSamples/sec; correspondingly, the overall two-sided frequency spacing is 64 GHz. The resolution of the DAC is assumed to be 8 bits. The peak to average power ratio is mitigated with a clipping ratio of 10 dB. Simulations were performed to confirm that using a DAC with fewer bits led to quantization noise that would have impaired performance. The DAC provides I and Q data outputs for the dual drive Mach Zehnder modulator (DDMZM). The DDMZM is modeled as in [3], and by a Gaussian transfer function whose bandwidth is adjusted for the scenario to be simulated. Indeed this transfer function is used to capture the bandwidth limitation of the channel.

The laser phase noise is modeled as a Wiener process with a specified linewidth $\Delta\nu$. The modulated light is propagated in fiber of a given length L using typical C-band characteristics: 16 ps/(nm×km) dispersion and 0.2 dB/km attenuation. The signal is photodetected (PD) and modeled as a square law device with additive white Gaussian noise (AWGN). The AWGN is meant to capture both thermal and shot noise and is included in the analysis in the $SNR_{k(RS)}$ term. An ideal analog to digital converter (ADC) is assumed for detection, i.e., no distortion. The receiver data is synchronized and the cyclic prefix is removed in the time domain. The signal is converted to the frequency domain via an FFT. After one-tap equalization the error vector magnitude (EVM) of each subchannel signal is calculated. Then the data is demodulated and the symbol error rate (SER) for each subchannel is calculated. Using EVM and SER we estimate SNR per subchannel (SNR estimation from EVM is valid for low EVM and SNR estimation from SER is accurate when the number of errors and EVM are high).

The estimated SNR from this Monte Carlo simulation is used to validate our theoretical expressions in section III. Once validated, theoretical expressions will be employed in sections IV and V for SSB-DMT.

APPENDIX B
SSBI CALCULATIONS

SSBI is the interference caused by subchannels beating with each other; it is independent of carrier power. This contribution can be shown to be

$$P_c\gamma^2\left(\left|\sum_{k=1}^{N} d_k e^{j[2\pi k\Delta f(t-T_k)+j\Phi(t-T_k)]}\right|^2-\left[\sum_{k=1}^{N}|d_k|^2\right]\right)$$
$$\approx 2P_cRe\left[\gamma^2\sum_{n=1}^{N}\sum_{\substack{m=1\\m\neq n}}^{N} d_n d_m^* e^{j2\pi(n-m))\Delta f t}\right], \tag{B.1}$$

where the interplay with phase noise and chromatic dispersion were neglected in the approximation, i.e., $T_k = 0$ and $\Phi(t) = 0$. To calculate the noise power per subchannel, consider the SSBI frequency domain representation. Each uniform SSB-DMT subchannel has an equal power delta function; square law detection is a convolution of the uniform SSB-DMT signal with itself in the frequency domain, so that $SSBI(f)$ is

$$\sum_{n=1}^{N}\sigma_{n(s)}^2\delta(f-n\Delta f) * \sum_{m=1}^{N}\sigma_{n(s)}^2\delta(f-m\Delta f) \tag{B.2}$$

The convolution yields the following result for an individual subcarrier

$$\sigma_{k(SSBI)}^2 = \sum_{n=-N}^{N}\sigma_{n(S)}^2\sigma_{k-n(S)}^2. \tag{B.3}$$

Recalling that $N\sigma_{n(S)}^2 = P_c\gamma^2$, we see that the sum of the variance per subchannel yields the total SSBI (B.1).

APPENDIX C
SER CALCULATION

The noise contributions in (17) are modeled as AWGN. Therefore, the SNR in a given subchannel determines its symbol error rate. When conditioned on a given phase rotation θ, the subchannel symbol error can be found via the complementary error function erfc. If the channel has a bandwidth limitation, the SNR_k is reduced by the channel filter (a Gaussian filter with 3 dB bandwidth of B) attenuation at that subchannel.

Points in a regular MQAM constellations have two, three or four nearest neighbors: more neighbors, higher SER. Points with two nearest neighbors (2NN) have SER_{2NN} given by

$$\int_{-\infty}^{\infty}\left[1-\left(\left[1-\frac{1}{4}\operatorname{erfc}\left(b\sqrt{SNR_k}\cos\left(\frac{\pi}{4}+\theta\right)\right)\right.\right.$$
$$\left.\left.-\frac{1}{4}\operatorname{erfc}\left(b\sqrt{SNR_k}\cdot\sin\left(\frac{\pi}{4}+\theta\right)\right)\right]\right)^2\Bigg] f_k(\theta)d\theta, \tag{C.1}$$

where b is the normalization factor of MQAM varying with M, and $f_k(\theta)$ is the probability density function of PR, a zero mean Gaussian with a variance of σ_{PR}^2.

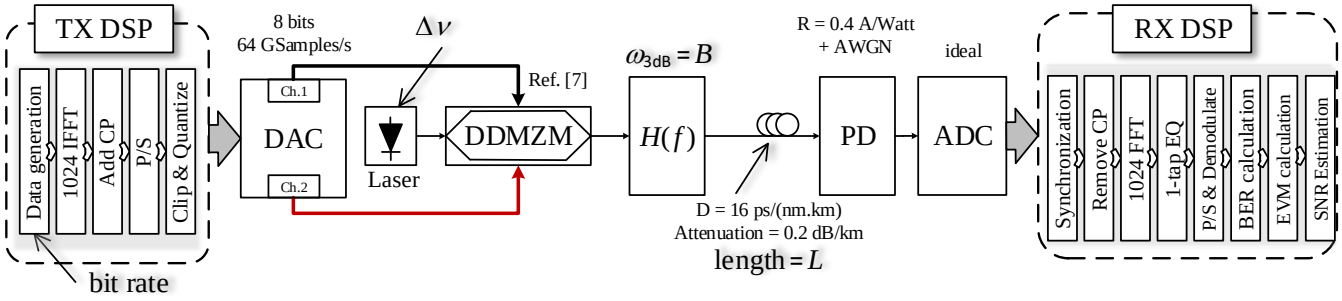

Fig. 8. Monte Carlo simulation block diagram and DSP flowchart for uniform SSB-DMT transmission.

For constellation points with three nearest neighbors (3NN) we have SER_{3NN} given by

$$\int_{-\infty}^{\infty}\left\{1-\left[1-\frac{1}{2}erfc\left(k\sqrt{\frac{2E_s}{N_0}}\cdot\cos\left(\frac{\pi}{4}+\theta\right)\right)-\frac{1}{2}erfc\left(k\sqrt{\frac{2E_s}{N_0}}\cdot\sin\left(\frac{\pi}{4}+\theta\right)\right)\right]\left[1-\frac{1}{4}erfc\left(k\sqrt{\frac{2E_s}{N_0}}\cdot\cos\left(\frac{\pi}{4}+\theta\right)\right)-\frac{1}{4}erfc\left(k\sqrt{\frac{2E_s}{N_0}}\cdot\sin\left(\frac{\pi}{4}+\theta\right)\right)\right]\right\}f(\theta)d\theta. \tag{C.2}$$

For constellation points with four nearest neighbors (3NN) we have SER_{4NN} given by

$$\int_{-\infty}^{\infty}\left\{1-\left[1-\frac{1}{2}\,\mathrm{erfc}\left(b\sqrt{SNR_k}\cdot\cos\left(\frac{\pi}{4}+\theta\right)\right)-\frac{1}{2}\,\mathrm{erfc}\left(b\sqrt{SNR_k}\cdot\sin\left(\frac{\pi}{4}+\theta\right)\right)\right]^2\right\}f(\theta)d\theta. \tag{C.3}$$

Finally the overall SER for MQAM is

$$SER_{MQAM}=\frac{1}{M}\sum_{i=1}^{M}SER_i. \tag{C.4}$$

where SER_i is replaced by SER_{jNN} for constellation point i with j nearest neighbors. Assuming Gray coding, the overall BER for MQAM is

$$BER_{MQAM}=\frac{1}{\log_2 M}SER_{MQAM}. \tag{C.5}$$

ACKNOWLEDGMENT

This research was sponsored by the Canadian Natural Sciences and Engineering Council under grants 170405 and 499664.

REFERENCES

[1] A. Yekani, M. Chagnon, C. S. Park, M. Poulin, D. V. Plant, and L. A. Rusch, "Experimental comparison of pam vs. dmt using an o-band silicon photonic modulator at different propagation distances," in *Optical Communication (ECOC), 2015 European Conference on*, Sept 2015, pp. 1–3.

[2] Y. Kai, M. Nishihara, T. Tanaka, R. Okabe, T. Takahara, J. C. Rasmussen, H. Ishihara, K. Goi, and K. Ogawa, "130-Gbps DMT transmission using silicon Mach-Zehnder modulator with chirp control at 1.55-m," in *Optical Fiber Communications Conference and Exhibition (OFC), 2015*, March 2015, pp. 1–3.

[3] L. Zhang, Q. Zhang, T. Zuo, E. Zhou, G. N. Liu, and X. Xu, "C-band single wavelength 100-Gb/s IM-DD transmission over 80-km SMF without CD compensation using SSB-DMT," presented at the Opt. Fiber Commun. Conf., Los Angeles, CA, USA, 2015, paper Th4A.2.

[4] W. R. Peng, "Analysis of Laser Phase Noise Effect in Direct- Detection Optical OFDM Transmission," *Journal of Lightwave Technology*, vol. 28, no. 17, pp. 2526–2536, Sept 2010.

[5] Z. Li, M. S. Erkln, K. Shi, E. Sillekens, L. Galdino, B. C. Thomsen, P. Bayvel, and R. I. Killey, "SSBI Mitigation and the Kramers-Kronig Scheme in Single-Sideband Direct-Detection Transmission With Receiver-Based Electronic Dispersion Compensation," *Journal of Lightwave Technology*, vol. 35, no. 10, pp. 1887–1893, May 2017.

[6] A. Mecozzi, C. Antonelli, and M. Shtaif, "Kramers–Kronig coherent receiver," *Optica*, vol. 3, no. 11, pp. 1220–1227, Nov 2016.

[7] Z. Li, M. S. Erk111n, R. Maher, L. Galdino, K. Shi, B. C. Thomsen, P. Bayvel, and R. I. Killey, "Two-Stage Linearization Filter for Direct-Detection Subcarrier Modulation," *IEEE Photonics Technology Letters*, vol. 28, no. 24, pp. 2838–2841, Dec 2016.

[8] X. Wang, J. Yu, Z. Cao, J. Xiao, and L. Chen, "SSBI mitigation at 60GHz OFDM-ROF system based on optimization of training sequence," *Opt. Express*, vol. 19, no. 9, pp. 8839–8846, Apr 2011.

[9] J. H. Yan, Y. W. Chen, B. C. Tsai, and K. M. Feng, "A Multiband DDO-OFDM System With Spectral Efficient Iterative SSBI Reduction DSP," *IEEE Photonics Technology Letters*, vol. 28, no. 2, pp. 119–122, Jan 2016.

[10] S. Randel, D. Pilori, S. Chandrasekhar, G. Raybon, and P. Winzer, "100-Gb/s discrete-multitone transmission over 80-km SSMF using single-sideband modulation with novel interference-cancellation scheme," in *2015 European Conference on Optical Communication (ECOC)*, Sept 2015, pp. 1–3.

[11] J. Ma, "Simple signal-to-signal beat interference cancellation receiver based on balanced detection for a single-sideband optical OFDM signal with a reduced guard band," *Opt. Lett.*, vol. 38, no. 21, pp. 4335–4338, Nov 2013.

[12] W. R. Peng, I. Morita, and H. Tanaka, "Enabling high capacity direct-detection optical OFDM transmissions using beat interference cancellation receiver," in *36th European Conference and Exhibition on Optical Communication*, Sept 2010, pp. 1–3.

[13] S. Yamamoto, N. Edagawa, H. Taga, Y. Yoshida, and H. Wakabayashi, "Analysis of laser phase noise to intensity noise conversion by chromatic dispersion in intensity modulation and direct detection optical-fiber transmission," *Journal of Lightwave Technology*, vol. 8, no. 11, pp. 1716–1722, Nov 1990.

[14] P. S. Chow, J. M. Cioffi, and J. A. C. Bingham, "A practical discrete multitone transceiver loading algorithm for data transmission over spectrally shaped channels," *IEEE Transactions on Communications*, vol. 43, no. 2/3/4, pp. 773–775, Feb 1995.